ISSN 0717-652X

COMPARISON OF BATHYMETRIC FEATURES DETECTED BY ERS2 SAR AND LANDSAT TM DATA OVER SAN MATÍAS GULF, ARGENTINA

Domingo A. Gagliardini, Ana I. Dogliotti, Haydée Karszenbaum & Francisco Grings

Instituto de Astronomía y Física del Espacio
Pabellón IAFE, Ciudad Universitaria, (1428) Buenos Aires, Argentina.
E-mail: agaglia@iafe.uba.ar

ABSTRACT

It is well known that Synthetic Aperture Radar (SAR) is capable of imaging bathymetric features by detecting changes in sea surface roughness associated with bathymetry-induced surface current modulations. The high dynamic range of LANDSAT Thematic Mapper (TM) and Enhanced TM+ (ETM+) sensors allow them to observe oceanic surfaces affected by solar specular reflection, or sun glint, without being saturated. This ability allows the imaging of sea surface roughness patterns in the sun glint affected area that are associated with surface current changes such as those produced by bathymetric features. ERS SAR and LANDSAT TM/ETM+ images obtained over the San Matías Gulf, Argentina during similar tidal current conditions are compared and the surface signature generated by the interaction of the tidal current with the bottom topography analyzed. Each type of sensor presents advantages and limitations to the observation of bottom features due to the way each one detects sea surface roughness. Still, when sun glint is present, TM/ETM+ and SAR show similar bathymetric patterns under the same tidal conditions. While both sensors provide consistent information over significant bathymetry features, increased differences in the detection is observed over weaker features.

INTRODUCTION

The observations provided by the Seasat-A satellite, launched in June 1978 by NASA, showed that the synthetic aperture radar (SAR) sensor could also serve as an efficient tool for detecting various types of sea bottom irregularities in the coastal zone. Many research works have further demonstrated this, among those produced in the last decade it can be mentioned Van der Kooij et al., 1995; Donato et al., 1997; Hesselman et al., 1997; Vogelzang, 1997; Johannessen, 2000; Gagliardini et al., 2004. Although SAR cannot provide detailed quantitative bathymetric measurements as those derived from acoustic methods, all of these works have shown that active microwave remote sensing can be used to provide a systematic and synoptic view of the bottom topography that may complement classical sounding observations. Fu and Holt (1982) and Henning et al. (1988) compared Sea SAT radar images with a return beam vidicom (RBV) scene and Skylab camera photograph respectively and they show that this two optical instrument, detecting sun glint radiation, can also provide useful information for sea bed topography studies. Recently, Gagliardini and Clemente Colón (2004a and 2004b) demonstrated the capability of LANDSAT TM images to identify ocean features generated by different ocean phenomena like changes in ocean currents generated by sea bed irregularities. They showed, by a qualitative comparison of this type of images and ERS-SAR data that over sun glint regions high-resolution optical sensors can provide observations of sea surface patterns related to ocean dynamic processes very similar to those captured by SAR. In this work, a comparison of LANDSAT ET/ETM+ and ERS 2 SAR data for sea bed forms detection is done and the differences between these two types of satellite information are discussed and also the advantages and disadvantages of each one are indicated. Imagery of the entrance of San Matías gulf, Argentina (Figure 1) is used. On this area, groups of sand waves were detected through acoustic records in the past (Servicio de Hidrografía Naval 1961, Pierce et al., 1969, Achilli and Aliotta 1992). Recently, Gagliardini et al. (2004a) using ERS-1 and ERS-2 information identified a large number of these type of bed forms, and obtained the first sand wave map of the region. In addition, a more complete map obtained as a result of processing (a series of LANDSAT TM/ETM+ images for the period 1997-2003 is presented in this paper.

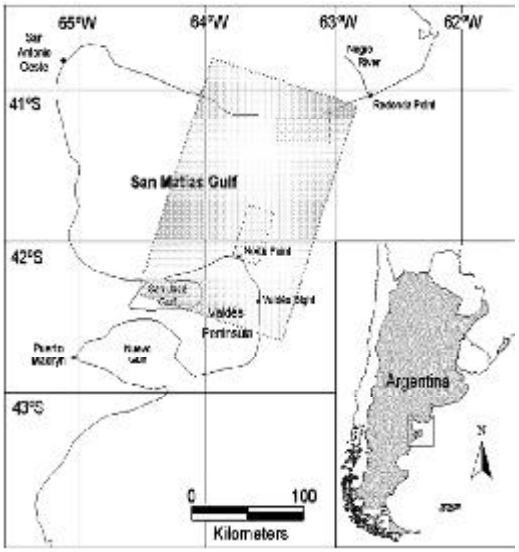

FIGURE 1: San Matías Gulf, the study area is indicated in clear grey.

STUDY AREA

The San Matías Gulf is located between 40º 47' S and 42º 13' S on the Atlantic coast of South America. It covers an area of approximately 17000 km^2 being the second largest gulf in Argentina. One of the most remarkable characteristics of this gulf is the presence of two large depressions exceeding 160 meters in depth in the middle of the gulf (Pierce et al., 1969). The sea bottom and sub-bottom in this region are made of fine-texture sediments unevenly deposited on the mid-upper Tertiary rock basement (Aliotta et al., 2000). On the eastern side, the continental shelf forms an open basin with a depth of about 60 meters at the entrance. Approximately 55% of the total gulf area exceeds 100 meters in depth (Piola and Scasso 1988).

The mouth of the Negro River is found to the northeast. It carries a substantial amount of fine sandy sediments to the coast, which are further carried eastward by littoral drift (Aliotta, 1983). At the gulf entrance, off the northeast coast of Valdés Peninsula, the bottom material is largely sandy. Large sand waves and broad undulations reported there (Achilli and Aliotta, 1992), added to the seismic configurations of the substratum (Aliotta et al., 2000), indicate intensive deposit-erosion processes and high sedimentary dynamics.

Semidiurnal tides govern the circulation inside the gulf. There are remarkable differences in tidal height amplitude along the coast. The mean height is 3 m at the mouth of the Negro River (gulf entrance) while it reaches 6 m in the inner region. Although current measurements are scarce, maximum tidal current values of the order of 2 m/s have been reported (Servicio de Hidrografía Naval Argentino, 1995). Monthly wind speed averages are of the order of 5 m/s in the coastal regions and 7 m/s in oceanic regions (Piola and Scasso, 1988).

SAR AND OPTICAL IMAGES

The SAR is a side-looking imaging radar operating from a moving platform (either satellite or aircraft). This sensor emits a series of microwave pulses toward the earth in a direction perpendicular to the flight path. Imagery is constructed from the strength and time delay of the returned signals, which depend primarily on the roughness and dielectric properties of the surface under observation and the distance to the radar. SAR images represent the spatial pattern of the intensity of the electromagnetic energy backscattered by the illuminated area. Over the ocean, SAR responds for the most to the surface roughness imposed by wind-generated capillary waves and small surface gravity waves (of the order of the radar wavelength, i.e. centimeters). According to Valenzuela (1978) resonance between the SAR pulses and these so-called Bragg waves is the major mechanism for the radar backscatter energy observed for incidence angles between 20º and 60º and for radar system with wave number kr and a incident angle $\emptyset$, the main contributor to the backscattered radar energy are ocean waves with wave number kb, given $kb = 2\,kr \sin\emptyset$. Thus, a SAR image of the ocean represents, to a first approximation, sea surface roughness conditions given by the spatial distribution of the wind-generated Bragg waves.

LANDSAT TM/ETM+ are passive sensors and their optical channels can be used to observe surface layer ocean color (upwelling radiance), and sun glint (reflected radiance) patterns of surface roughness. The upwelling radiance depends on the scattering and absorption processes of sun radiation in the water mass. In the case of sun glint it depends on the ocean reflectance mechanism that can be explained by physical optics. This theory applies provided $kr\,? > 1$, where ? is the local curvature radius of the rough ocean surface (Rufenach and Smith 1985). Namely the curvature radius of the water facet,

which is inclined so as to reflect an incoming ray from the sun toward the optical sensor, should be larger than the wavelength.

Therefore, an optical image from the ocean represents the spatial pattern of the intensity of the electromagnetic energy composed by the two indicated components. According to Gagliardini and Clemente Colón (2004a) when the solar illumination geometry favors the observation of the upwelling radiance over sun glint (low solar elevation and azimuth angles) TM channels 1, 2 and 3 can provide information related to water constituents in the upper ocean layer. On the other hand, when sun glint is present (November to February) it dominates over the upwelling water-leaving radiance detected by the TM sensor. Additionally, since sun glint is relatively weakly dependent on wavelength, surface features delineated by strong sun glint can be observed in all optical bands, this is not the case for the upwelling radiance, which is detected only by the visible bands.

The imaging mechanism for microwaves is different from the optical one, however, both types of processes obviously depend on the presence of small gravity and capillary waves. Thus, the intensity of the detected radiation depends on the sea surface roughness conditions, increasing or decreasing when the roughness, that is, when wind velocity, augments or diminishes. It depends also on the radiation frequency, and it will decrease when the channel wavelength increases.

MATERIAL AND METHODS

ESA ERS satellites, that carries SAR sensor, have a Sun-synchronous, near polar, quasi-circular orbit with a mean altitude of 785 km and an inclination of 98.5º. The SAR is a C-band instrument (5.3 GHz) that illuminates the ground with a 100 km wide swath from which 100 km x 100 km frames or images with a resolution of approximately 25 m are produced. This right-looking radar collects data in ascending and descending orbits and has a repeat cycle period of 37 days.

LANDSAT TM and ETM+ satellites were launched in an heliosynchronic orbit with 8 days' shift. The TM sensor has 7 spectral bands with 30 m spatial resolution, except the thermal channel with 120 m. The wavelengths associated with each channel are : 0.45-0.52 mm (blue), 0.52-0.60 mm (green), 0.63- 0.69 mm (red), 0.76-0.90 mm (close IR), 1.55-1.75 mm (medium IR), 2.08-2.35 mm (middle IR) and 10.40 - 12.50 mm (thermal IR). The ETM+ sensor has 7 very similar bands but with significant radiometric improvements. Moreover, a panchromatic channel has been added (0.52-0.90 mm) with 15 m spatial resolution and the thermal channel resolution has been increased to 60 m. In both cases the swath width is approximately 185 km for each orbit.

A set of approximately 15 LANDSAT TM/ETM+ images, corresponding to Path 227 and Row 89, obtained between November and January, for the period 1997-2003 were analyzed. As a first step in the processing, a radiometrically corrected and map oriented image level 5 ETM+ image was selected, and georreferenced in the Gauss Kruger projection (Transverse Mercator) using ground coastal land and landcontrol points previously measured determined with a GPS device. Next, the remaining images were co-registered to the previous one in order to compare the information provided by each of them. Then, the land was masked using channel 7 in order to isolate the water and highlight the observed patterns. ERS-SAR frames, combined in mosaics used by (used in Gagliardini et al., (2004), were also available and co-registered to LANDSAT images.

Tidal records at Norte point were obtained and the tidal current direction associated with each image was extracted from tidal reports. Table 1 shows the tidal stage at Norte Point, the most relevant location for this work. Meteorologica Meteorological observations for the region were only available at the Puerto Madryn airport, 120 km away from Norte

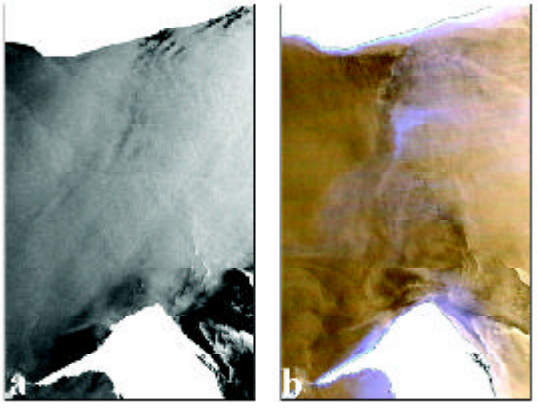

FIGURE 2: General view of the study area observed by SAR (a) and TM (b), indicated in clear grey in Figure 1.

Point. Unfortunately, wind speed and direction data acquired at Puerto Madryn are not necessarily representative of the conditions over the area of the critical features here analyzed because of the distance and the large area under study.

RESULTS

To show a general view of the study region, in figure 2, a mosaic constructed with the first ERS-1 SAR frames taken over the area on July 9, 1992 and a subset of LANDSAT-ETM+ images (channels 4, 3 and 2) of the same area, obtained on January 23, 2000 are presented. In figure 3, SAR and optical close-up images of the area near Norte Point, corresponding to October 5, 1997 and January 17, 2002, respectively, are presented. A series of bright and dark linear features, caused by the interaction of the tide current with sand waves (Gagliardini et al 2004), can be clearly noticed in both images. The direction of the tidal flow at the entrance of the gulf (middle point), inferred from the tidal charts, is also shown. It can be seen that both types of images present the same features with the same sequence of dark and bright patterns along the linear features when the tidal current has the same direction. This sequence is inverted when the tidal current is inverted. In figures 4a and 4b, SAR and optical close-up images of the north area are presented. It can be noted that in this case, the patterns observed are not the same and they are not as well defined as those found in the southern area. This difference was noted in all the images analyzed. That is, both the SAR and TM data sets processed showed more differences in the observations of features in the northern area than in the southern, where the same linear structures always appears at the same tidal conditions.

A sand wave map was drawn digitizing the linear features observed in the LANDSAT images (figure 5a). The sand wave map drawn by Gagliardini et al. (2004) using ERS-SAR images is shown in figure 5b. By comparing both maps it can be observed that there are no differences in the southern area but it is clear that the first map is more complete, it shows more features in the northern area of the gulf's entrance.

For a quantitative comparison both images were calibrated, that is, count values were transformed into reflectance values at the top of the atmosphere, for the optical data, and into backscattering coefficient in decibels (s^0) for the SAR data. Images were also co-registered to be able to compare the same areas. Transects over the same area in both type of images were drown perpendicular to de sand waves, first in the south region where the linear features are easily observed and then in the north where they are more diffuse. In the first case, the difference in reflectance generated by the sand wave is clearly observed in all bands. In figure 6a, this transect is presented and the corresponding reflectance values for TM channel 3 is shown as an example. It can be observed that the reflectance changes approximately from 0.022 to 0.038 due to the presence of the sand dune. For this channel gain and bias and illumination conditions, one count value corresponds to 0.0015 in reflectance. Therefore, it can be considered that this change is radiometrically detectable. In figure 6b the same area and the same transect for SAR data is presented. Opposed tidal current was selected to show that a similar linear feature is generated, but with the dark-clear sequence inverted. It can be noted that in this case the change it is not detectable due to the radiometric uncertainty generated by speckle. The only way to detect it is by filtering the image with a median filter, which increases the number of looks and diminishes the uncertainty, but in this case, spatial resolution is reduced. Median filters of 3x3, 5x5 y 7x7 were applied. The results obtained for the last case are presented in figure 6b showing that after image filtering, the change in dB for the same sand wave is detectable taken a value of approximately 10 dB.

In the case of sand waves not easily observed, as it is in the northern area, the transect drawn, shows that not only SAR data cannot detect the generated linear features, but also the optical data. Although these linear features are clearly visible in the screen and can be digitized, they cannot be detected numerically because in these cases the change in dB and the change in reflectance values are of the order of the background noise. This fact shows that the human eyes have a great ability in detecting spatial structures which favors the construction of a sand dune map of the complete study area.

DISCUSSION ANND CONCLUSION

Wind speeds between 3 and 12 m/sec provide the roughness patterns required for the observation of most ocean features in SAR and optical sensors generating capillary and small surface gravity waves

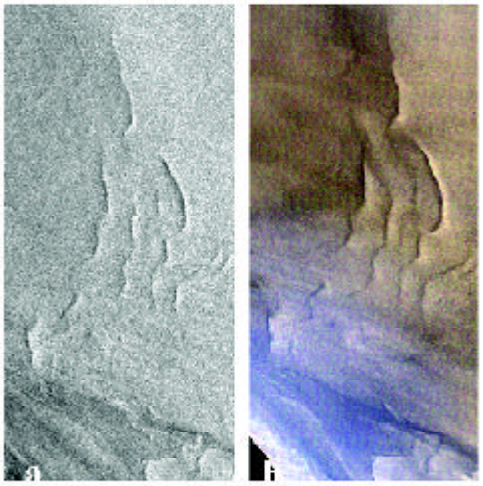

FIGURE 3: Linear patterns observed by SAR (a) and TM (b) at the south area (indicated in dark grey in Figure 1).

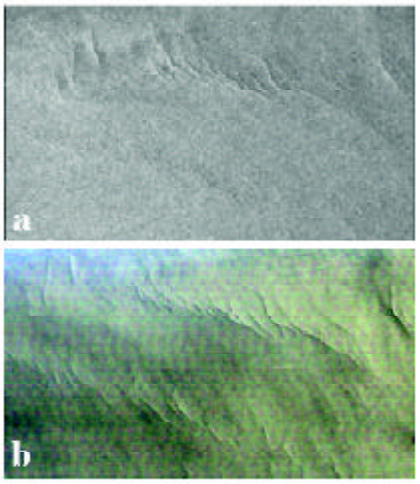

FIGURE 4: Linear patterns observed by SAR (a) and TM (b), in the north area (indicated in dark grey in Figure 1).

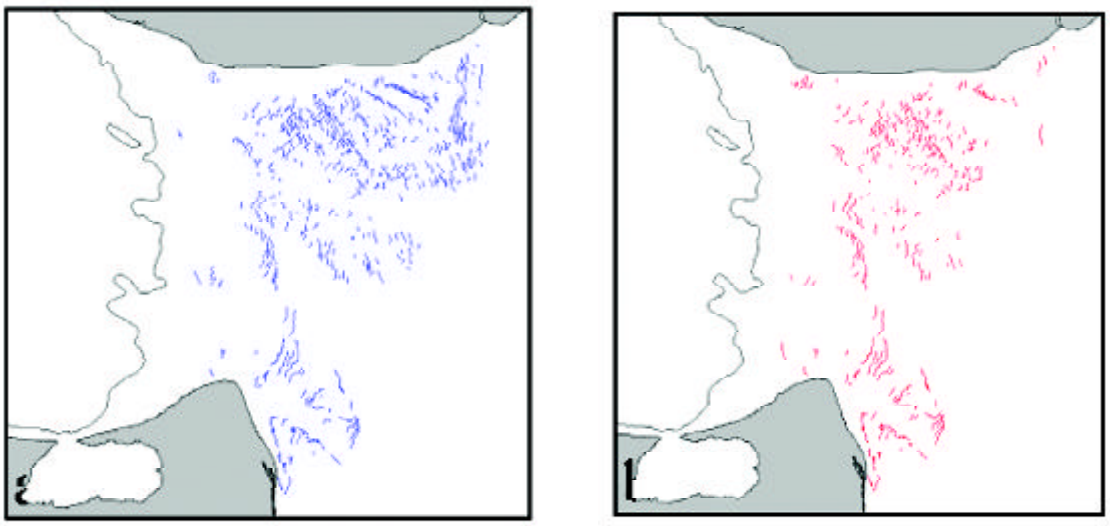

FIGURE 5: a) Sand waves detected with TM data and b) sand waves detected with SAR data.

(of the order of a centimeter). Thus, SAR and sun glint images of the sea represent, to a first approximation, sea surface roughness conditions given by the spatial distribution of this type of waves. The distinct signatures produced by the modulation of capillary and short surface gravity waves by ocean circulation are most evident under these limits. At much lower wind speeds, the wave effects decrease producing a smoother sea surface that reflects energy away from the sensors resulting in dark areas in the SAR imagery. At higher wind speed, the affected area is characterized by significant background clutter that diminishes the contrast of ocean signatures imaged. In the same way, current speeds above 0.4 –0.5 m/sec (Shuchman et al., 1985; Vogelzand et al., 1992) are necessary to detect bottom topography and higher speeds, that increase the surface roughness, will facilitate sea bed forms detection. Also, it is necessary to take into account that, for a sand wave to be detected it is necessary that its height would be significant with respect to the depth (McLeish et al., 1981). Only under this condition the change in ocean currents will modify the distribution of Bragg waves facilitating the

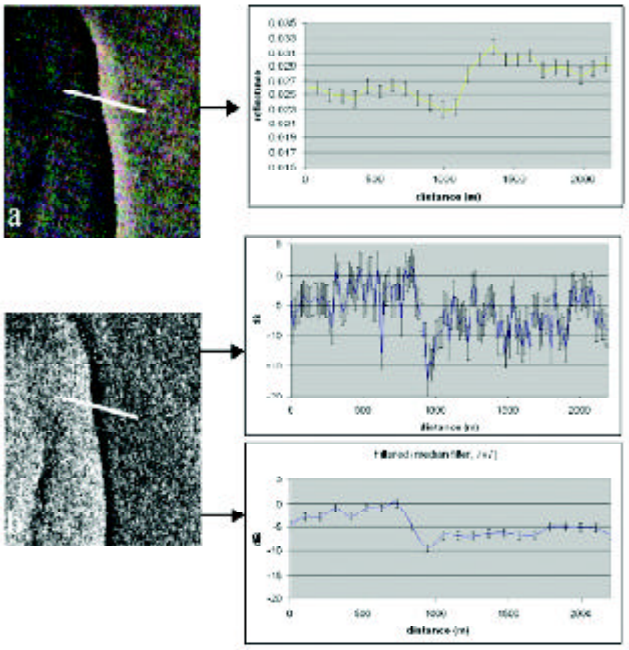

FIGURE 6: a) transect over a TM image and the corresponding reflectance values, b) the same transect over the same area in a SAR image and the corresponding dB values non filtered and filtered 7x7

observation of bottom topography.

In the study area, according to Gagliardini et al. (2004), the necessary wind, current speed and sand wave height are adequate to detect the generated change in the surface roughness. However, taking into account that sand waves were not consistently captured over the entire gulf entrance region in the available set of images, particularly in the northern area, it is necessary to consider that these conditions were not fulfilled all the time. This may have been in part due to the variability of the wind field over the extensive area covered by the observations. Wind velocities should not be expected to be necessarily uniform over the entire region and at times may reach values outside the optimum interval needed to image these features. In addition, tidal currents, that are much intense in the southern area than in the north (Gagliardini et al., 2004), can have uneven velocities over the gulf entrance and depend on the tidal stage at the time of the observation.

The sun glint intensity strongly depends on the observation angle of the sensor (Henning et all, 1994) and, in the case of LANDSAT, this values range between + 5.5 º along the scan line. At the time of the satellite passage (10:30 AM, local time) the sun is located at the right side of the observed area and the maximum intensity is detected at the right side of the image, strongly decreasing to the left side. In this way, in general, ocean processes seen by this type of phenomenon can be clearly observed, only on the right side of the image. This situation favors the detection of sand waves in the study area because the entrance of San Matías gulf is located at the right side of the frame 227-89. Meanwhile, it is necessary to take into account that sun glint is also strongly dependent upon the sun position (Henning et all, 1994, Gagliardini and Clemente Colón 2004a), therefore on sun illumination geometry that changes during the day and along the year for each point of the ocean surface. Due to this fact, it is necessary to consider that the San Matías gulf is located quite south (42º S 64º W) and the solar elevation angle in the summer solstice (December 21st) is 51º approximately and the sun glint intensity would be much lower than in the northern region, such us the one studied by Gagliardini and Clemente Colón (2004a), where the elevation angle in the summer solstice is 58º approximately.

According to the quantitative results obtained it is possible to say that speckle masks the signal generated by the sand wave in the SAR images of the entrance of San Matías gulf. After filtering the image this signal can be radiometrically measured but this implies a decrease in spatial resolution. This

could be done in the southern area where the linear features are stronger. In the case of optical images it is only possible to detect the features in the south region, even though the sun glint signal can be evaluated without filtering. In spite of the fact that the structures cannot be radiometrically detected in northern area, they can visually be observed and this is due to the capability of the human eyes to detect spatial patterns, like the ones generated by the sand waves.

Consistent with the previous points, it can be said that SAR as well as TM images can provide information on the bottom geomorphology at the entrance of San Matías gulf. But it is necessary to consider that:

TM has the limitations of any optical sensor including the need for cloud-free conditions and daylight.

TM ability depends on sun glint conditions and is limited to high solar azimuth and zenith angle months (October to March), while SAR sand dune features are observable all year around.

ERS-1 SAR images can detect surface roughness features across the full swath width of an image while TM observations are restricted to the right-hand side of the image that is impacted by the strongest sun glint conditions.

Although having similar spatial resolution, TM optical images do not suffer from speckle noise characteristic of coherent SAR observations, allowing a better observation of weaker features.

In regions where signatures are stronger both, TM and SAR data, provide similar observations of the bathymetric conditions while where signatures are weaker TM data results to be more sensitive.

·In regions were signatures are weak the noise in both type of images are higher than the difference in signal generated by the sea bed irregularity and they cannot be radiometrically detected. Investigation on specific spatial filters that enhance these features could be very useful for an automatic identification of sand waves.

Therefore, it can be said that each type of sensor presents advantages and limitations to the observation of bottom features due to the way each one detects sea surface roughness. Still, when sun glint is present TM/ETM+ and SAR show similar bathymetric patterns under the same tidal conditions. While both sensors provide consistent information over significant bathymetry features, increased differences between them are detected over weaker features. In this regard, the more complete map, obtained as a result of processing 1997-2003 LANDSAT TM/ETM+ images, demonstrated that high resolution optical images to be especially useful, independently or as a complement to side-scanning techniques in the identification and mapping of sand waves.

ACKNOWLEDGEMENTS

The authors are grateful to the Argentine Comisión Nacional de Actividades Espaciales (CONAE) for providing the LANDSAT-TM/ETM+ and ERS-SAR data used in this work.

REFERENCES

ACHILLI, S.M. & ALIOTTA, S., 1992. Características morfológicas de ondas de arena de la plataforma continental al sur de la provincia de Buenos Aires, Argentina. *Proceedings of the 3as Jornadas Geológicas Bonaerenses* (La Plata, Buenos Aires, Argentina), 207-212. [1]

ALIOTTA, S., 1983. Estudio sedimentológico y de deriva litoral entre la desembocadura del Río Negro y Playa Bonita (Pcia. de Río Negro). *Univ. Nac. del Sur -Instituto Argentino de Oceanografía*, Grad. Degree Thesis, 58p. [2]

ALIOTTA, S., KOSTADINOFF, J. & LIZASOAIN, G., 2000. Sísmica somera con 3,5 kHz de la Plataforma Continental norpatagónica, Argentina. Proceedings of II Congreso Latinoamericano de Sedimentología , 29-30. [3]

DONATO, T.F.; ASKARI, F.; MARMORINO, G.O.; TRUMP, C.L., & LYZENGA D.R., 1997. Radar imaging of sand waves on the continental shelf east of Cape Hatteras, NC, U.S.A. *Continental Shelf Research*, Vol. 17 , 9, 989-1004. [4]

FU, L.-L. & HOLT, B., 1982. Seasat Views Ocean and Sea Ice with Synthetic Aperture Radar, *NASA/JPL Publication* 81-120. [5]

GAGLIARDINI, D.A., ALIOTTA, S. DOGLIOTTI, A. & CLEMENTE COLÓN, P., 2004. Identification of bed forms trough ERS SAR images in San Matías gulf, Argentina. Accepted in Journal of Coastal Research. [6]

GAGLIARDINI, D.A. & CLEMENTE COLÓN, P. 2004A. A comparative assessment on the use of SAR and high-resolution optical image in ocean dynamics studies. *International Journal of Remote Sensing*, Vol., 25, 7-8, 1271-1275. [7]

GAGLIARDINI D.A. & CLEMENTE COLÓN, P., 2004B. Ocean feature detection using microwave backscatter and sun glint observations, *presented also in this Meeting.* [8]

HESSELMAN, C., CALKOEN & WENSINK, H., 1997. Mapping on seabed topography to and from SAR. *Proceeding of the Third ERS Symposium, Space at the Service of Our Environment, ESA Publ. Div.* ESA SP-414,

pp 1055-1058. [9]

HENNINGS, I., DOERFFER, R. & ALPERS, W., 1988 Comparison of submarine relief features on a radar satellite image and a Skylab satellite photograph. International Journal of Remote Sensing. Vol. 9-1, 45-67. [10]

HENNINGS, I., J. MATTHEWS & M. METZNER, 1994. Sun glitter radiance and radar cross-section modulations of the sea bed, *Journal of Geophysical Research*, Vol.99-8, 16.303-16.326. [11]

JOHANNESSEN, J.A.,2000. Coastal observing systems: the role of Synthetic Aperture radar. *Johns Hopkins APL, Technical Digest*, Vol. 21, 41-48. [12]

MCLEISH, W.; SWIFT, D.J.; LONG, R.B.; ROSS, D. & MERRIL, G., 1981. Ocean surface patterns above sea-floor bedforms as recorded by radar, southern bight of North Sea. *Marine Geology*, 43, M1-M8. [13]

PIERCE, J.W.; SIEGUEL, F.R., & URIEN, C.M., 1969. Topografía submarina del Golfo San Matías. *Proceedings of the VI Jornadas Geológicas Argentinas (Buenos Aires, Argentina).* Actas III, pp.127-140. [14]

PIOLA, A. & SCASSO, L.M., 1988. Circulación en el Golfo San Matías. *GEOACTA*, Vol. 15-1, 33-51. [15]

RUFENACH, C. & SMITH, C. 1985. Observation of internal waves in Landsat and SEASAT satellite imagery, *Inernationl. Journal of Remote Sensing*, Vol. 6-7, 1.201-1.207. [16]

SERVICIO DE HIDROGRAFÍA NAVAL ARGENTINO, 1961. Dunas gigantes en el Golfo San Matías, Rep. Argentina *Documento del Servicio De Hidrografía Naval* (H622). 2p. [17]

SERVICIO DE HIDROGRAFIA NAVAL ARGENTINO, 1995. *Carta batimétrica H214 (Golfo San Matías y San José).* Scale 1:275,000, Mercator Projection, 1 sheet. [18]

SHUCHMAN, R.A.; LYZENGA, D.R., & MEADOWS, G.A., 1985. Synthetic Aperture radar imaging of ocean-bottom topography via tidal-current interactions: theory and observations. *International Journal of Remote Sensing*, Vol. 6-7, 1179-1200. [19]

VALENZUELA, G.R., 1978. Theory for the interaction of electromagnetic and ocean waves, a review. *Boundary Layer Meteorol.* 13, 61-85. [20]

VAN DER KOOIJ, M., VOGELZANG, J., & CALCOEN, C., 1995.A simple analytical model for brightness modulations caused by submarine sand waves in radar imagery. *Journal of Geophysical Research*, Vol. 100, 7069-7082. [21]

VOGELZANG J.; WENSINK, G.J.; DE LOOR, G.P.; PETERS, H.C., & POUWELS, H., 1992. The mapping of bottom topography with x-band slar: the relation between radar imagery and bathymetry. *International Journal of Remote Sensing*, Vol. 13, 1943-1958. [22]

VOGELZANG, J. 1997. Mapping submarine sand waves with multiband imagine radar 1. Model development and sensitivity analysis. *Journal of Geophysical Research*, Vol. 102 (C1), 1163-1181. [23]